PNAS RESEARCH ARTICLE | MEDICAL SCIENCES OPEN ACCESS

# Distinct and opposite effects of leukemogenic *Idh* and *Tet2* mutations in hematopoietic stem and progenitor cells

Jerome Fortin[a,1,2], Ming-Feng Chiang[a,1], Cem Meydan[b,c,d,3], Jonathan Foox[b,c,3], Parameswaran Ramachandran[a,3], Julie Leca[a], François Lemonnier[a,e], Wanda Y. Li[a,f], Miki S. Gams[g], Takashi Sakamoto[a,h], Mandy Chu[a], Chantal Tobin[a], Eric Laugesen[a], Troy M. Robinson[i,j], Annick You-Ten[a], Daniel J. Butler[b], Thorsten Berger[a], Mark D. Minden[a], Ross L. Levine[i,k,l], Cynthia J. Guidos[g], Ari M. Melnick[m], Christopher E. Mason[b,c,d], and Tak W. Mak[a,f,n,2]

Contributed by Tak W. Mak; received May 24, 2022; accepted December 12, 2022; reviewed by Timothy J. Ley and Ravindra Majeti

**Mutations in *IDH1, IDH2*, and *TET2* are recurrently observed in myeloid neoplasms. *IDH1* and *IDH2* encode isocitrate dehydrogenase isoforms, which normally catalyze the conversion of isocitrate to α-ketoglutarate (α-KG). Oncogenic *IDH1/2* mutations confer neomorphic activity, leading to the production of D-2-hydroxyglutarate (D-2-HG), a potent inhibitor of α-KG-dependent enzymes which include the TET methylcytosine dioxygenases. Given their mutual exclusivity in myeloid neoplasms, *IDH1, IDH2*, and *TET2* mutations may converge on a common oncogenic mechanism. Contrary to this expectation, we observed that they have distinct, and even opposite, effects on hematopoietic stem and progenitor cells in genetically engineered mice. Epigenetic and single-cell transcriptomic analyses revealed that $Idh2^{R172K}$ and *Tet2* loss-of-function have divergent consequences on the expression and activity of key hematopoietic and leukemogenic regulators. Notably, chromatin accessibility and transcriptional deregulation in $Idh2^{R172K}$ cells were partially disconnected from DNA methylation alterations. These results highlight unanticipated divergent effects of *IDH1/2* and *TET2* mutations, providing support for the optimization of genotype-specific therapies.**

IDH | TET2 | myeloid neoplasm | epigenetics

## Significance

In myeloid neoplasms, treatment outcome is associated with the presence of specific combinations of driver mutations. Delineating their molecular effects is important to understand the basis of disease heterogeneity and to help design better therapies. We discovered that two mutually exclusive leukemogenic mutations, $Idh2^{R172K}$ and *Tet2* loss-of-function, unexpectedly cause opposite molecular alterations in hematopoietic stem and progenitor cells. These results could pave the way for the development of more effective and patient-specific treatments.

Myeloid neoplasms are characterized by the altered proliferation and aberrant differentiation of immature myeloid cells (1). Within this disease spectrum, acute myeloid leukemia (AML) has the worst prognosis, which is heavily influenced by the underlying genetics (1–4). In many cases, AML emerges from myelodysplastic syndrome (MDS) or myeloproliferative neoplasm (MPN) transformation, occasionally preceded by clonal hematopoiesis (CH) (1, 5).

Alterations in epigenetic regulators are found in a large proportion of myeloid neoplasms and AML (6). Among these, missense mutations in the genes encoding isocitrate dehydrogenase-1 and -2 (*IDH1* and *IDH2*) are observed in around 20% of AML and 5 to 10% of MDS and MPN (3, 4, 6, 7). These mutations cause substitutions at arginine 132 (R132) in IDH1, at the equivalent residue (R172) in IDH2, or at R140 in IDH2 (3, 4, 8–11). Canonically, wild-type IDH1/2 catalyzes the reversible conversion of isocitrate into α-ketoglutarate (α-KG) (8). Mutant IDH1/2 gains neomorphic enzymatic activity, reducing α-KG to D-2-hydoxyglutarate (D-2-HG) (11, 12), a potent inhibitor of several dioxygenases that normally use α-KG as a cofactor (13, 14). Among those enzymes are the ten-eleven translocation (TET) family of methylcytosine dioxygenases, which hydroxylate 5-methylcytosine (5-mC) bases in the DNA to generate 5-hydroxymethylcytosine (5-hmC) (13, 15).

*TET2* is mutated in 15 to 30% of MDS or MPN and 10 to 20% of AML (3, 4, 15–20). *TET2* and *IDH1/2* lesions are mutually exclusive and display an overlapping hypermethylated phenotype (3, 4, 13, 21). In the rare instances where both occur in the same tumor, they are most often in distinct subclones (22, 23). Thus, the oncogenic effect of D-2-HG in hematopoietic cells could be mainly attributable to the inhibition of *TET2*. However, several observations argue against a simple equivalence of *IDH1/2* and *TET2* mutations. First, D-2-HG can alter the activity of multiple α-KG-dependent dioxygenases beyond TET family members, including several histone demethylases and prolyl hydroxylases, thus potentially affecting a larger spectrum of cellular processes (8, 14, 24). Second, *TET2* mutations are frequent in CH, whereas *IDH1/2* lesions are much rarer, suggesting distinct effects on hematopoietic stem cell (HSC) fitness or differences in time to progression to more overt disease (5, 25, 26). Third, while *TET2* and *IDH2* mutations are mutually exclusive in AML, they frequently co-occur in a distinct malignancy, angioimmunoblastic T cell lymphoma (AITL), pointing to cell context-dependent interplay between them (27, 28). Fourth, divergent patterns of co-occurring lesions are observed in AML with *TET2* versus *IDH1/2* mutations (3, 4). Nevertheless, it remains unclear whether these differences reflect non-overlapping or altogether opposite molecular effects of *IDH1/2*

Author contributions: J.Fortin, M.-F.C., C.M., J.Foox, P.R., J.L., F.L., W.Y.L., T.S., D.J.B., T.B., M.D.M., R.L.L., C.J.G., A.M.M., C.E.M., and T.W.M. designed research; J.Fortin, M.-F.C., C.M., J.Foox, P.R., J.L., F.L., W.Y.L., M.S.G., T.S., M.C., C.T., E.L., T.M.R., and A.Y.-T. performed research; M.D.M. contributed new reagents/analytic tools; J.Fortin, M.-F.C., C.M., J.Foox, P.R., F.L., M.S.G., T.S., C.J.G., A.M.M., and C.E.M. analyzed data; and J.Fortin., M.D.M., R.L.L., C.J.G., A.M.M., C.E.M., and T.W.M. wrote the paper.

Reviewers: T.J.L., Washington University in St Louis School of Medicine; and R.M., Stanford University School of Medicine.

Competing interest statement: The authors declare competing interest. The authors have organizational affiliations to disclose, T.W.M. is a consultant for AstraZeneca and Tessa Therapeutics., Yes, the authors have stock ownership to disclose, T.W.M. owns equity in Treadwell Therapeutics Inc. and Agios Pharmaceuticals., Yes, the authors have research support to disclose, T.W.M. has unrelated research funding from AstraZeneca.



[1]J.Fortin. and M.F.C. contributed equally to this work as first authors.

[2]To whom correspondence may be addressed. Email: jerome.fortin@uhnresearch.ca, tak.mak@uhnresearch.ca, or tmak@uhnres.utoronto.ca.

[3]C.M., J.Foox., and P.R. contributed equally to this work as second authors.

This article contains supporting information online at https://www.pnas.org/lookup/suppl/doi:10.1073/pnas.2208176120/-/DCSupplemental.

Published January 18, 2023.

and *TET2* lesions. Adding further complexity, there are apparent differences between *IDH1/2* mutations (3, 4, 29), possibly related to the level of D-2-HG production (30) or to isoform-specific cellular localization (IDH1 in cytoplasm versus IDH2 in mitochondria).

IDH inhibitors have shown success in the treatment of AML (31–33), but the description of resistance mechanisms highlights the need to better understand the oncogenic mechanism of action of *IDH1/2* mutations and to develop improved genotype-specific treatments (34–37). Toward this goal, we set out to delineate the cellular effects of distinct *IDH1* and *IDH2* mutations and how they may differ from *TET2* loss-of-function, by performing phenotypic, transcriptomic, and epigenomic analyses of hematopoietic stem and progenitor cells in genetically engineered mice.

## Results

**Graded Hematopoietic Effects of *Idh1/2* Mutations in Knock-in Mice.** To directly compare the effects of $Idh1^{R132H}$, $Idh2^{R140Q}$, and $Idh2^{R172K}$ on hematopoiesis, we crossed mice carrying the *Cre*-inducible $Idh1^{LSL\text{-}R132H}$, $Idh2^{LSL\text{-}R140Q}$, and $Idh2^{LSL\text{-}R172K}$ knock-in alleles with *Vav-Cre* transgenic animals, thus activating the mutations in hematopoietic stem and progenitor cells. The recombination efficiency of all three alleles was similar (*SI Appendix*, Fig. S1*A*). Mice expressing the knock-in alleles displayed elevated levels of D-2-HG in the circulation and in lineage-negative ($Lin^-$) bone marrow cells (Fig. 1 *A* and *B*), which were much higher in $Idh2^{R172K}$ mice than in $Idh1^{R132H}$ and $Idh2^{R140Q}$ animals. These differences, which are in line with previously reported data from engineered cell lines (30), are unlikely to be due to technical variations between the similarly constructed mutant alleles. Indeed, while *Idh2* was modestly upregulated in $Idh2^{R172K}$ cells, this was primarily attributable to increased relative expression of the wild-type allele, probably due to homeostatic feedback (*SI Appendix*, Fig. S1*B*). Consistently, total IDH2 protein levels were elevated in $Idh2^{R172K}$ cells (*SI Appendix*, Fig. S1*C*).

$Idh2^{R172K}$ mice succumbed to lethal hematopoietic disease with a median latency of 324 d (Fig. 1*C*). $Tet2^{-/-}$ mice showed a milder phenotype, with a median survival of 448 d matching previous reports (Fig. 1*C*) (38–41). Most (~60%) of the diseased $Idh2^{R172K}$ mice exhibited overt MDS/MPN, and a smaller proportion developed lymphoid malignancies (Fig. 1*D* and *SI Appendix*, Fig. S2 *A* and *B*). Animals with myeloid disease displayed splenomegaly, peripheral leukocytosis, anemia, and blasts in the circulating blood (Fig. 1 *E* and *F*). In the bone marrow, $CD11b^+Gr1^+$ myeloid cells were expanded, while $CD71^+Ter119^+$ erythroid progenitors were depleted (Fig. 1*G*). Concomitantly, the enlarged spleens exhibited disrupted architecture and contained a high proportion of myeloid and erythroid cells (Fig. 1 *E* and *G*). The spleens also harbored a substantial population of hematopoietic $Lin^-Sca1^+cKit^+$ (LSK) progenitors (Fig. 1*G*), which included some LSK $CD150^+CD48^-$ long-term hematopoietic stem cells (LT-HSCs), indicative of extramedullary hematopoiesis (*SI Appendix*, Fig. S2*C*). LSK cell expansion was also noted in the bone marrow (Fig. 1*G*). Similar myeloproliferative diseases were occasionally observed in aging $Idh1^{R132H}$ and $Idh2^{R140Q}$ mice (*SI Appendix*, Fig. S2*D*). Targeted sequencing using the M-IMPACT assay detected very few additional variants, of uncertain significance, in $Idh2^{R172K}$ MDS/MPN (*SI Appendix*, Fig. S2E and Dataset S1).

Complete blood count analysis indicated neutropenia, lymphopenia, and anemia as early as 3 mo of age in $Idh2^{R172K}$ animals (*SI Appendix*, Fig. S3*A*). Erythrocyte mean corpuscular volume (MCV) was also increased in $Idh2^{R172K}$ mice, suggesting dysplasia. $Idh1^{R132H}$ and $Idh2^{R140Q}$ mice were largely normal across all the measured parameters, although both exhibited mild increases in erythrocyte MCV (*SI Appendix*, Fig. S3*A*). In addition, older $Idh2^{R140Q}$ mice showed moderate lymphopenia (*SI Appendix*, Fig. S3*A*). Overall, these results indicate that under otherwise identical genetic conditions, distinct *Idh1/2* mutations differ substantially in their phenotypic consequences: $Idh2^{R172K}$ causes progressive hematopoietic defects, evolving to overt myeloid or lymphoid neoplasms, while $Idh2^{R132H}$ and $Idh2^{R140Q}$ have much milder effects.

**$Idh2^{R172K}$ and *Tet2* Loss of Function Differentially Affect Hematopoietic Stem and Progenitor Cells.** To better understand the effects of *Idh1/2* mutations on early hematopoiesis, we examined the stem and progenitor cell compartments in the bone marrow of 3 to 9-mo-old mice. $Idh2^{R172K}$ mice displayed increased percentages of $Lin^-cKit^+Sca1^-$ (LK) erythromyeloid progenitor, as well as $Lin^-cKit^+Sca1^+$ (LSK) stem and early progenitor cells (Fig. 2 *A* and *B* and *SI Appendix*, Fig. S3*B*). Within the LSK compartment, $Idh2^{R172K}$ mice had normal abundance of $CD150^-CD48^-$ multipotent progenitors (MPPs), but increased percentages of slightly more committed $CD150^-CD48^+$ HPC-1 and $CD150^+CD48^+$ HPC-2 progenitors and decreased $CD150^+CD48^-$ LT-HSCs (Fig. 2*C* and *SI Appendix*, Fig. S3*B*). This was confirmed using alternative markers, CD34 and Flt3 (Fig. 2*D*). Within the LK compartment, $Idh2^{R172K}$ animals had elevated percentages of $CD34^+CD16/32^{mid}$ common myeloid progenitors (CMP) and $CD34^+CD16/32^+$ granulocyte/monocyte progenitors (GMPs), whereas $CD34^-CD16/32^-$ megakaryocyte/erythroid progenitors (MEPs) were decreased, indicating myeloid skewing (Fig. 2*E*). Overall, $Idh2^{R172K}$ animals somewhat differed from *Tet2*-deficient mice, which have increased LSK cells and progenitors but normal numbers of LT-HSCs, as previously reported (39, 40, 42, 43) and confirmed here (*SI Appendix*, Fig. S3*C*). $Idh1^{R132H}$and $Idh2^{R140Q}$ mice did not substantially differ from control littermates (Fig. 2 *B–E* and *SI Appendix*, Fig. S3*B*).

To confirm and extend our flow cytometric assessment, we examined stem and progenitor cells in the bone marrow of healthy 4-mo-old mutant and control mice using time-of-flight mass cytometry (CyTOF) (*SI Appendix*, Fig. S4 *A–D*). Results for the major stem and progenitor subsets across the LK and LSK compartments were consistent with the data obtained by fluorescent flow cytometry (*SI Appendix*, Fig. S4 *A* and *B*). We further dissected the progenitor subsets by separating the LSK cells based on the expression of Flt3, which distinguishes lymphoid-biased ($Flt3^+$) from myeloid-biased ($Flt3^-$) progenitors. $Flt3^+$ LSK cells were increased in $Idh2^{R172K}$ mice (Fig. 2*F* and *SI Appendix*, Fig. S4*A*). This population can be divided between IL7R-$\alpha^-$ lymphoid-biased progenitors and slightly more differentiated IL7R-$\alpha^+$ committed lymphoid precursors (CLP). CyTOF analyses indicated increased $Flt3^+$ IL7R-$\alpha^-$ LSK progenitors, but decreased CLPs in $Idh2^{R172K}$ animals, suggesting a differentiation block during lymphoid commitment (Fig. 2*F*). Consistent with the lower number of MEPs observed in $Idh2^{R172K}$ mice, $Ter119^+CD71^+$ and $CD71^+CD45^{lo}$ erythroblasts were significantly reduced (*SI Appendix*, Fig. S4*C*). $Idh1^{R132H}$ and $Idh2^{R140Q}$ mice were largely noral across all the parameters evaluated (*SI Appendix*, Fig. S4 *B* and *C*). To assess whether changes in stem and progenitor subsets in $Idh2^{R172K}$ mice could be explained by abnormal proliferation, we pulse-labeled cells in vitro with Iodo-deoxy-uridine (IdU) prior to CyTOF analysis. The frequency of $IdU^+$ cells was either unchanged (in LT-HSCs, MPPs, and erythroblasts) or decreased (in $Flt3^-$ HPC-1s and HPC-2s, and in erythromyeloid progenitors) (Fig. 2*G* and *SI Appendix*, Fig. S4 *D* and *E*). Collectively, these results indicated that alterations in progenitor numbers in $Idh2^{R172K}$ mice were not accompanied by corresponding changes in proliferation and likely reflect impaired differentiation (Fig. 2*H*).

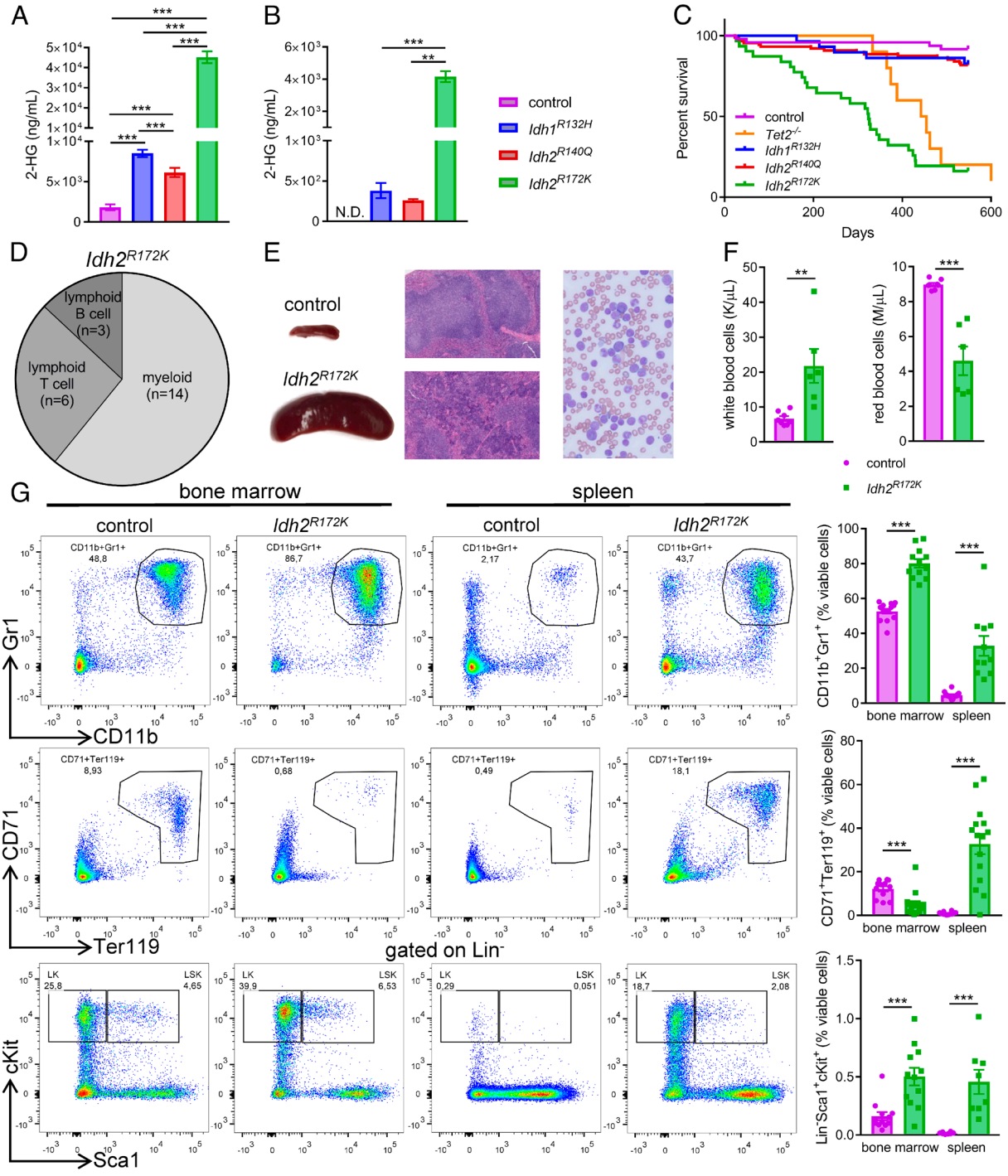


**Fig. 1.** (*A* and *B*) Level of D-2-HG in the blood (*A*) and lineage-negative cells (*B*) isolated from 3 to 9-mo-old mice with the indicated genotypes. In panel *A*, n = 68 to 272 per genotype. In panel *B*, n = 4 per genotype. (*C*) Kaplan–Meier curves depicting the survival of mice with the indicated genotypes. (*D*) Disease classification of *Idh2*$^{R172K}$ mice at humane endpoint, based on flow cytometry analysis. (*E*) Representative spleen (*Left*), H&E-stained spleen histological section (*Center*) and peripheral blood smear (*Right*) of *Idh2*$^{R172K}$ and control mice at endpoint. (*F*) Counts of circulating white blood cells and red blood cells in *Idh2*$^{R172K}$ mice exhibiting myeloid neoplasms, and in their control littermates, at humane endpoint. Each dot represents an individual animal. (*G*) Representative flow cytometry plots and quantification of CD11b$^{+}$Gr1$^{+}$ myeloid cells, CD71$^{+}$Ter119$^{+}$ erythroid cells, and Lin$^{-}$cKit$^{+}$Sca1$^{+}$ hematopoietic progenitors in the bone marrow and spleen of *Idh2*$^{R172K}$ mice exhibiting myeloid neoplasms and of their control littermates, at humane endpoint. Each dot represents an individual animal. Data were analyzed using ANOVA with Tukey post hoc tests (*A* and *B*) and *t* tests (*F* and *G*). $^{**}P < 0.01$; $^{***}P < 0.001$.

To evaluate whether stem and progenitor alterations affected their self-renewal potential, we measured the colony-forming ability of bone marrow cells in serial replating assays in methylcellulose medium containing cytokines (IL-3, IL-6, SCF, and EPO). While control bone marrow cells exhibited a much-reduced capacity to form new colonies by the fourth plating, *Idh2*$^{R172K}$ cells retained colony-forming potential through at least eight replatings (*SI Appendix*, Fig. S4*F*). *Idh1*$^{R132H}$ and *Idh2*$^{R140Q}$ cells preserved some ability to yield colonies through five and six platings, respectively (*SI Appendix*, Fig. S4*F*). Given that *Idh2*$^{R172K}$, but not *Tet2*$^{-/-}$, causes a depletion of the LT-HSCs in vivo (*SI Appendix*, Fig. S3*C* and Refs. 39, 40, and 42), we asked whether the two

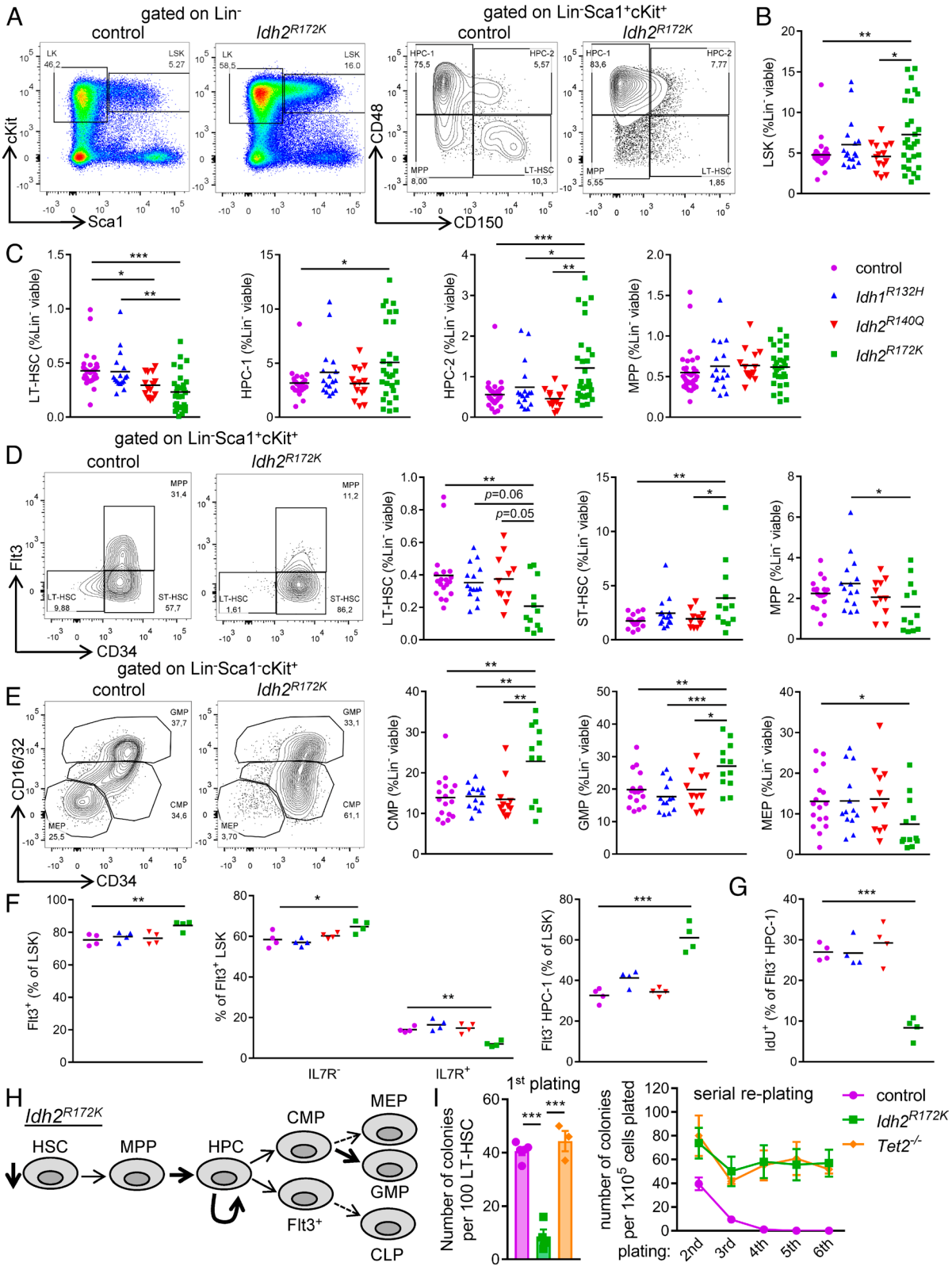


**Fig. 2.** (*A*) Representative flow cytometry plots depicting the gating strategy to identify Lin$^-$cKit$^+$Sca1$^+$ (LSK) hematopoietic progenitors and their subsets of long-term hematopoietic stem cells (LT-HSCs), multipotent progenitors (MPPs), and hematopoietic progenitor cells (HPC-1 and HPC-2) in the bone marrow of *Idh2*$^{R172K}$ and control mice. (*B*) Quantification of LSK cells in the bone marrow of 3 to 9-mo-old mice with the indicated genotype. Each dot represents an individual mouse. (*C*) Quantification of LT-HSC, HPC-1, HPC-2, and MPP cells in the bone marrow of 3 to 9-mo-old mice with the indicated genotype. Each dot represents an individual mouse. (*D*) Representative flow cytometry plots and quantification of LSK subsets divided based on Flt3 and CD34 immunoreactivity to identify LT-HSCs, short-term hematopoietic stem cells (ST-HSCs), and MPPs in the bone marrow of 3 to 9-mo-old mice with the indicated genotypes. Each dot represents an individual animal. (*E*) Representative flow cytometry plots and quantification of Lin$^-$cKit$^+$ (LK) erythromyeloid progenitor subsets (common myeloid progenitors, CMP; granulocyte/monotype progenitors, GMP; megakaryocyte/erythroid progenitor, MEP) in the bone marrow of 3 to 9-mo-old mice with the indicated genotypes. Each dot represents an individual animal. (*F*) Proportion of LSK cells immunoreactive for Flt3, of Flt3$^+$LSK cells immunoreactive for IL7R, and of HPC-1 cells negative for Flt3, in the bone marrow of mice with the indicated genotype, assessed by CYTOF. Each dot represents an individual animal. (*G*) Proportion of Flt3$^-$HPC-1 cells positive for iododeoxyuridine (IdU) in the bone marrow of mice with the indicated genotype, assessed by CyTOF. Each dot

mutations differentially affect HSC functionality in vitro. In contrast to *Tet2*$^{-/-}$, sorted *Idh2*$^{R172K}$ LT-HSCs were profoundly impaired in their initial colony-forming potential (Fig. 2*I*). However, *Tet2*$^{-/-}$ and *Idh2*$^{R172K}$ cells showed similarly enhanced serial replating ability through at least six passages (Fig. 2*I*). These data suggest that *Idh2*$^{R172K}$ and *Tet2*$^{-/-}$ both enhance progenitor self-renewal but have distinct effects on HSC fitness.

**Transcriptomic Effects of *Idh2*$^{R172K}$ Revealed by scRNA-seq.** To investigate the molecular basis for differences between the *Idh1/2* and *Tet2* mutants on hematopoietic stem and progenitor cells, we analyzed the transcriptome of LSK cells from young adults (before any overt disease onset) +/+;*Vav-Cre* (WT), *Idh1*$^{R132H}$, *Idh2*$^{R140Q}$, *Idh2*$^{R172K}$, and *Tet2*$^{-/-}$ mice. t-SNE analysis indicated that *Idh2*$^{R172K}$ and *Tet2*$^{-/-}$ cells robustly clustered away from controls and from each other (Fig. 3*A*). By contrast, *Idh1*$^{R132H}$ and *Idh2*$^{R140Q}$ samples intermingled with controls (Fig. 3*A*). Most of the differentially expressed genes in *Idh2*$^{R172K}$ and *Tet2*$^{-/-}$ cells did not overlap (Fig. 3*B*), with many showing opposite trends compared with WT (*SI Appendix*, Fig. S5*A*). In agreement with our flow cytometry analyses, Gene Set Enrichment Analysis (GSEA) indicated that *Idh2*$^{R172K}$ and *Tet2*$^{-/-}$ cells downregulated markers of hematopoietic progenitor differentiation and proliferation but showed opposite alterations of genes associated with HSCs and early progenitors (*SI Appendix*, Fig. S5*B*).

To examine the transcriptomic changes driven by mutant IDH1/2 with more granularity, we performed single-cell RNA-seq on LSK cells isolated from *Idh1/2* mutant mice and their WT controls (*SI Appendix*, Fig. S6*A*). Clustering using Seurat, and visualization by t-SNE and UMAP, revealed that *Idh2*$^{R172K}$ cells robustly segregated from the other genotypes (Fig. 3*C*). *Idh1*$^{R132H}$, *Idh2*$^{R140Q}$, and WT cells remained intermingled even when reclustered in the absence of *Idh2*$^{R172K}$ cells (*SI Appendix*, Fig. S6 *B* and *C*), consistent with another *Idh2*$^{R140Q}$ mouse model (44). Eleven "normal" clusters comprising mostly *Idh1*$^{R132H}$, *Idh2*$^{R140Q}$, and WT cells were functionally annotated using marker genes and SCENIC (45) to predict transcription factor activity. These analyses identified HSCs/early progenitors (*Gata2*, *Hlf*, *Meis1*, and *Procr*), erythroid-biased progenitors (*Gata1*, *Pbx1*, *Stat5,* and *Tal1*), myeloid-biased progenitors (*Cebpb*, *Ctsg*, *Mpo*, and *Irf8*), lymphoid-biased progenitors (*Dntt*, *Il7r*, *Ikzf1*, and *Klf3*), transitory MPPs, and proliferative (activated) cells (*E2f3*, *E2f8*, *mKi67*, and *Top2a*) (Fig. 3*D* and *SI Appendix*, Fig. S6*D*).

We next examined the four clusters that contained almost exclusively *Idh2*$^{R172K}$ cells. The largest (*Idh2*$^{R172K}$ Prog.1) expressed high levels of the HSC-enriched genes *Gata2* and *Kit* (*SI Appendix*, Fig. S6*E*). SCENIC indicated that these cells had features of HSCs and early progenitors but aberrantly upregulated *Runx1*- and *Sox4*-driven gene expression programs (Fig. 3*D*). This was also seen in another *Idh2*$^{R172K}$-specific cluster (*Idh2*$^{R172K}$ Prog.2) (Fig. 3*D*), which further upregulated modulators of self-renewal and differentiation (e.g., *Cdk6*, *Pim1*, *Notch2*, and *Kdm6b*) (*SI Appendix*, Fig. S6 *D* and *E*). Accordingly, this cluster uniquely combined transcription factor activities seen in HSCs and activated progenitors (Fig. 3*D*). Thus, *Idh2*$^{R172K}$ Prog.1, and *Idh2*$^{R172K}$ Prog.2 likely represent quiescent and activated/self-renewing abnormal early progenitors, respectively. A third *Idh2*$^{R172K}$-specific cluster (*Idh2*$^{R172K}$ Prog.3) segregated from other cell populations by t-SNE analysis but expressed few unique markers (*SI Appendix*, Fig. S6 *D* and *E*). An "*Idh2*$^{R172K}$ lymphoid" cluster highly expressed markers of lymphoid-primed progenitors (e.g., *Dntt*, *Il12a*, *Il7r*, and *Flt3*) (*SI Appendix*, Fig. S6 *D* and *E*) and aberrantly upregulated *Runx1*- and *Sox4*-driven transcriptional programs (Fig. 3*D*).

The above results suggested that *Idh2*$^{R172K}$ disrupts hematopoietic stem and progenitor differentiation. To investigate this possibility further, we used Slingshot (46) to predict cell differentiation trajectories, using HSCs as the starting point. This analysis inferred lineage paths flowing through early and transitory progenitors and branching off to terminate in lymphoid-biased (Lineage 2), myeloid-biased (Lineage 5), erythroid-biased (Lineage 3), and activated cell clusters (Lineage 1) (Fig. 3*E* and *SI Appendix*, Fig. S7*A*). Two additional trajectories comprising mostly *Idh2*$^{R172K}$ cells were observed: one terminated within the activated/self-renewing *Idh2*$^{R172K}$ Prog.2/3 clusters (Lineage 4) and the other within the large population of abnormal quiescent cells forming the *Idh2*$^{R172K}$ Prog.1 cluster (Lineage 6) (Fig. 3*E* and *SI Appendix*, Fig. S7*A*). These data, together with the marker and transcription factor activity analyses described above, are consistent with impaired differentiation of early *Idh2*$^{R172K}$ progenitors.

***Tet2*-Deficient and *Idh2*$^{R172K}$ Abnormal Early Progenitors Are Transcriptionally Different.** To understand in more detail how *Tet2*$^{-/-}$ and *Idh2*$^{R172K}$ LSK cells transcriptionally differ, we combined our single-cell transcriptomic results with a published dataset from Lin$^-$ *Tet2*$^{flox/flox}$;*Mx1-Cre* (hereafter, *Tet2*$^{-/-}$) bone marrow cells (44). Data integration using Seurat (47), and iterative clustering, indicated that WT cells from the two studies largely intermingled, whereas *Idh2*$^{R172K}$ cells clustered separately, as expected (Fig. 3*F*). Interestingly, around 40% of the *Tet2*$^{-/-}$ cells formed a population that segregated from both control and *Idh2*$^{R172K}$ cells (cluster 7 in Fig. 3*F*). Marker and SCENIC analyses indicated that these cells represented early progenitors, downstream of HSCs (Fig. 3*G*). Differential gene expression analysis between this cell population and WT early progenitors indicated relatively modest differences but was notable for upregulation of the myeloid oncogene and hematopoietic self-renewal driver *Myb* (48–50) and downregulation of the HSC/progenitor regulator *Lmo2* and of the AP-1 family transcription factors *Fos* and *Junb* in *Tet2*$^{-/-}$ cells (*SI Appendix*, Fig. S7*B*). Overall, bulk and single-cell studies indicated distinct effects of *Tet2* and *Idh2*$^{R172K}$ mutations on the transcriptome of LSK cells.

**Distinct and Opposite Chromatin Accessibility Changes Induced by *Idh2*$^{R172K}$ and *Tet2*$^{-/-}$.** Given that D-2-HG inhibits histone lysine demethylases and TET methylcytosine dioxygenases, we next examined epigenetic alterations in *Idh1/2* and *Tet2* mutated cells. We first profiled chromatin accessibility in LSK cells by ATAC-seq. As seen with RNA-seq, *Idh2*$^{R172K}$ samples profoundly differed from the other genotypes, corresponding to a large number of differentially accessible loci (Fig. 4 *A* and *B* and *SI Appendix*, Fig. S8). *Tet2*$^{-/-}$ samples also diverged from WT but showed fewer significant changes (Fig. 4 *A* and *B* and *SI Appendix*, Fig. S8). *Idh1*$^{R132H}$ and *Idh2*$^{R140Q}$ cells did not display robust alterations (Fig. 4*B* and *SI Appendix*, Fig. S8). In *Idh2*$^{R172K}$ and *Tet2*$^{-/-}$ cells, differences in gene expression correlated

represents an individual animal. (*H*) Schematic summarizing hematopoietic progenitor alterations in *Idh2*$^{R172K}$ mice. Thicker and dashed lines represent differences from wild type. (*I*) Number of colonies generated in primary plating of LT-HSCs sorted from mice with the indicated genotype (*Left*), and in subsequent serial replating (*Right*), in M3434 methylcellulose medium. N = 3 to 5 mice per genotype. Data were analyzed with ANOVA and Tukey (*B–E* and *I*) or Dunnett (*F* and G, with +/+;*Vav-Cre* mice being the control group) post hoc tests. *$P$ < 0.05; **$P$ < 0.01; ***$P$ < 0.001.

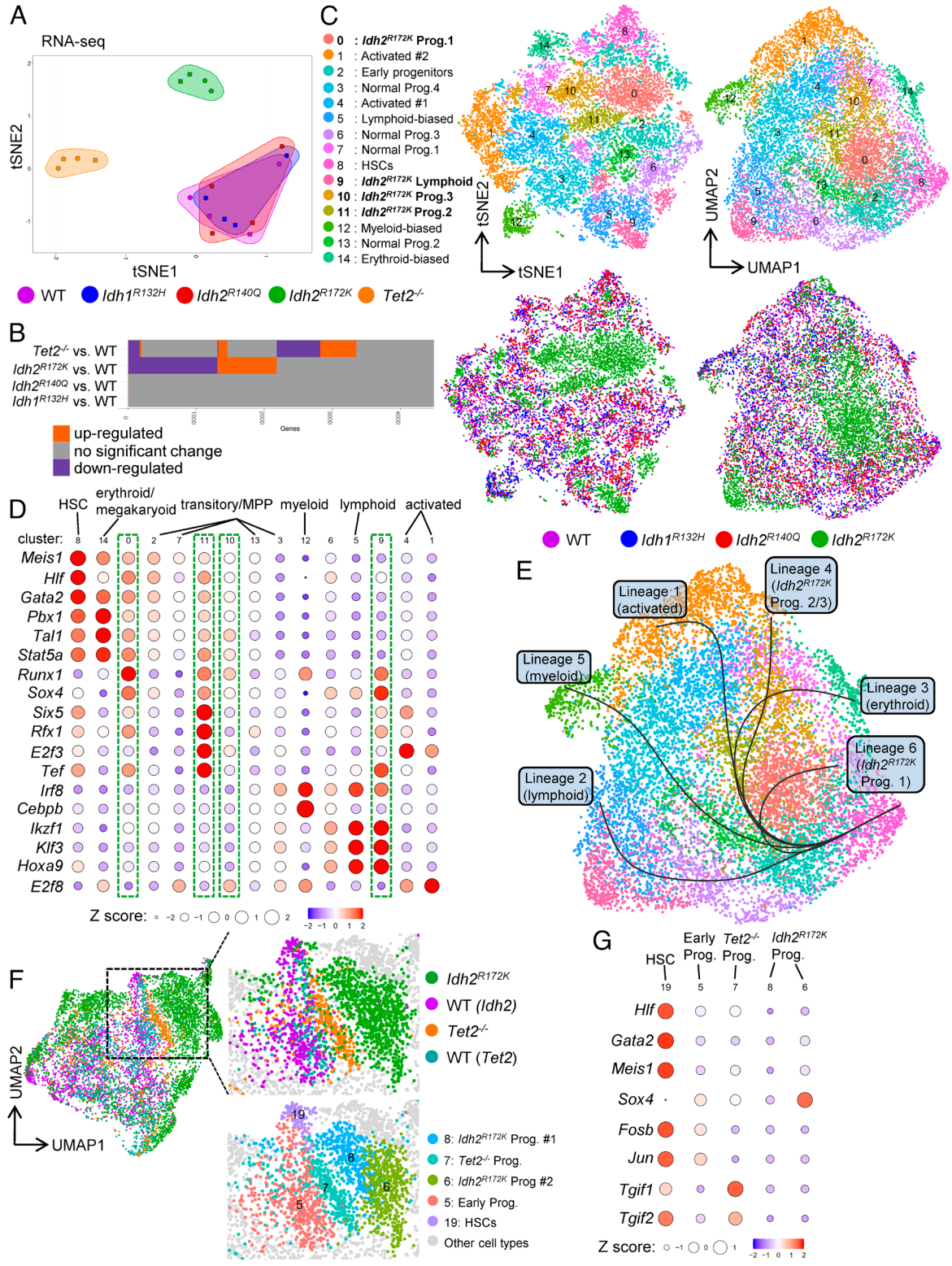


**Fig. 3.** (*A*) t-SNE plot depicting the similarity in overall transcriptional profile of bone marrow LSK cells isolated from mice with the indicated genotypes, based on RNA-sequencing analysis. Each dot represents an independent sample (biological replicate), each derived from cells pooled from two mice. (*B*) Plot depicting significantly upregulated and downregulated genes in LSK cells with the indicated genotypes, compared with +/+;*Vav-Cre* (WT) cells. (*C*) t-SNE and UMAP representations of bone marrow LSK cells from mice with the indicated genotypes, clustered based on the similarity of their transcriptome determined by scRNA-seq. Cells are colored according to their Seurat-identified cluster number and genotype. (*D*) SCENIC analysis of transcription factor regulon activity in the Seurat-identified clusters depicted in panel *C*. The Z score of regulon activity in each cluster, calculated relative to the average regulon activity in all the clusters, is represented by the size and color scale of the dots. (*E*) Slingshot-predicted differentiation trajectories, starting from HSCs, overlaid on top of the UMAP clustering of LSK cells shown in panel *C*. (*F*) UMAP representation of bone marrow cells from mice with the indicated genotypes, clustered based on the similarity of their transcriptome determined by scRNA-seq. WT (+/+;*Vav-Cre*) and *Idh2*$^{R172K}$ cells are from the LSK samples shown in panel *C*. WT (+/+;*Mx1-Cre*) and *Tet2*$^{-/-}$ (*Tet2*$^{flox/flox}$;*Mx1-Cre*) cells are from a previously published dataset of Lin$^{-}$ bone marrow cells. Clustering was performed following iterative rounds of data integration as described in the *Methods* section. Clusters of interest are emphasized. (*G*) SCENIC analysis of transcription factor regulon activity in the Seurat-identified clusters depicted in the inset in panel *F*. The Z score of regulon activity in each cluster, calculated relative to the average regulon activity in all the clusters, is represented by the size and color scale of the dots.

with changes in chromatin accessibility near gene promoters (*SI Appendix*, Fig. S9*A*). We next examined previously identified active LSK enhancers, marked by H3 acetylated on lysine 27 (H3K27ac) and methylated on lysine 4 (H3K4me1) (51). Nearly all the significantly altered LSK enhancers in *Tet2*$^{-/-}$ cells were closing (109/110; 99%— Fig. 4*B* and Dataset S2). In striking contrast, *Idh2*$^{R172K}$ cells harbored a mixture of opening (691/2,461; 28%) and closing (1,770/2,461; 72%) enhancers (Fig. 4*B* and Dataset S2). For example, *Idh2*$^{R172K}$-specific upregulation of *Gata2* and *Meis1* was associated with increased accessibility of known regulatory elements (52–56) (Fig. 4 *C*–*E*). By contrast, downregulation of the HSC

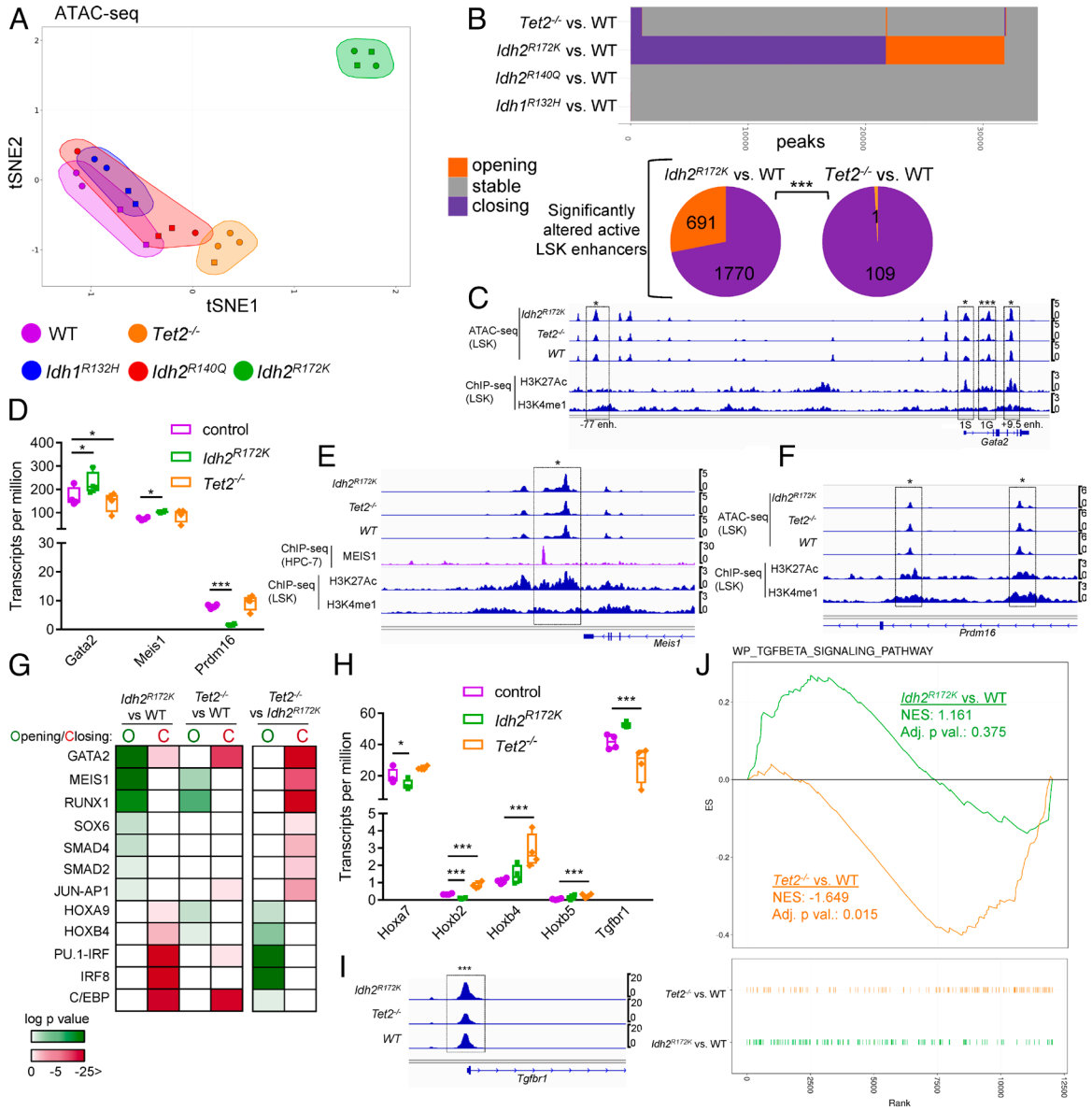


**Fig. 4.** (*A*) t-SNE plot depicting the similarity in overall chromatin accessibility profile of LSK cells isolated from mice with the indicated genotypes, based on ATAC-seq analysis. Each dot represents an independent sample (biological replicate), each derived from cells pooled from two mice. (*B*) *Top*: Plot depicting loci with significantly higher or lower chromatin accessibility in LSK cells with the indicated genotypes, compared with *+/+;Vav-Cre* (WT) cells. *Bottom*: proportion of significantly altered LSK enhancers that are opening and closing in *Idh2*$^{R172K}$ and *Tet2*$^{-/-}$ cells. Data were analyzed by a chi-square test with Yates correction. (*C*) ATAC-seq tracks representing the normalized average chromatin accessibility near the *Gata2* gene in LSK cells isolated from mice with the indicated genotypes. Tracks depicting the levels of H3K27ac and H3K4me1, derived from published chromatin immunoprecipitation experiments in LSK cells, were aligned to the ATAC-seq tracks. Differentially accessible peaks of interest are boxed. (*D*) Relative expression of the indicated genes, determined by bulk RNA-seq analysis, in LSK cells isolated from mice with the indicated genotypes. Each dot represents an individual sample. (*E*) ATAC-seq tracks representing the normalized average chromatin accessibility near the *Meis1* gene in LSK cells isolated from mice with the indicated genotypes. Tracks depicting MEIS1, H3K27ac, and H3K4me1 occupancy at an autoregulatory enhancer (boxed), derived from published chromatin immunoprecipitation experiments in LSK and HPC-7 cells, were aligned to the ATAC-seq tracks. (*F*) ATAC-seq tracks representing the normalized average chromatin accessibility near the *Prdm16* gene in LSK cells isolated from mice with the indicated genotypes. Tracks depicting the levels of H3K27ac and H3K4me1, derived from published chromatin immunoprecipitation experiments in LSK cells, were aligned to the ATAC-seq tracks. A differentially accessible peak of interest is boxed. (*G*) Enrichment of the indicated transcription factor binding motifs at loci gaining (opening) or losing (closing) chromatin accessibility in LSK cells isolated from mice with the indicated genotype. *P* values are indicated using a color scale, which was truncated at log *P* = −25 for clarity. (*H*) Relative expression of the indicated genes, determined by bulk RNA-seq analysis, in LSK cells isolated from mice with the indicated genotypes. Each dot represents an individual sample. (*I*) ATAC-seq tracks representing the normalized average chromatin accessibility near the *Tgfbr1* gene in LSK cells isolated from mice with the indicated genotypes. (*J*) GSEA plot depicting the relative expression of TGFβ signaling pathway genes in *Idh2*$^{R172K}$ and *Tet2*$^{-/-}$ LSK bone marrow cells, compared to their wild-type counterparts, based on RNA-sequencing data.

modulator *Prdm16* (57–59) in *Idh2*$^{R172K}$ cells was accompanied by chromatin closing near the promoter and within an intronic enhancer (51) (Fig. 4*F*).

To identify potential regulatory networks affected in *Idh2*$^{R172K}$ and *Tet2*$^{-/-}$ cells, we probed the differentially accessible chromatin regions for known transcription factor binding sites. *Gata2*, *Runx1*, *Meis1*, and *Sox* motifs were enriched at chromatin opening loci in *Idh2*$^{R172K}$ cells (Fig. 4*G*), matching the SCENIC analysis of single-cell transcriptomic data (Fig. 3*D*). In contrast, motifs for positive regulators of myeloid maturation, such as *Spi1/Pu.1*, *Irf8*, and *Cebp*, were enriched at sites of chromatin closing (Fig. 4*G*), as seen near the promoter of the mature myeloid marker *Fcer1g* (*SI Appendix*, Fig. S9*B*). As in *Idh2*$^{R172K}$ cells, *Runx1* and *Meis1* motifs significantly opened in *Tet2*$^{-/-}$ cells, albeit more modestly (Fig. 4*G*). In striking opposition to *Idh2*$^{R172K}$ cells, *Gata2* motifs were enriched in closing chromatin sites in *Tet2*$^{-/-}$ cells (Fig. 4*G*), accompanied by a mild downregulation of *Gata2* expression (Fig. 4*D*). *Hox* binding sites gained accessibility in *Tet2*$^{-/-}$ cells compared with *Idh2*$^{R172K}$ cells, tracking with *Tet2*$^{-/-}$-specific upregulation of several *Hox* family transcription factors (Fig. 4 *G* and *H*). Potentially relevant for these observations, *NPM1* mutations, which are strongly associated with *Hox* gene upregulation, co-occur with *Tet2*, *Idh1*$^{R132}$, and *Idh2*$^{R140}$ but are mutually exclusive with *Idh2*$^{R172}$ mutations in AML (3, 60). Conversely, *AP-1* and *Smad*-bound loci had decreased accessibility in *Tet2*$^{-/-}$ cells (Fig. 4*G*). For *AP-1*, this was consistent with the lower transcriptional activity of FOS and JUN in early *Tet2*$^{-/-}$ progenitors in single-cell data (Fig. 3*G*). Closing of binding sites for SMAD2/4, the canonical effectors of TGFβ signaling, was associated with *Tet2*$^{-/-}$-specific down-regulation of *Tgfbr1*, decreased accessibility of the *Tgfbr1* promoter, and increased activity of the SMAD2 transcriptional corepressors, *Tgif1/2*, predicted by SCENIC in single *Tet2*$^{-/-}$ progenitors (Figs. 3*G* and 4 *H* and *I*). Accordingly, GSEA indicated that TGFβ signaling was downregulated in *Tet2*$^{-/-}$ compared with WT and *Idh2*$^{R172K}$ cells (Fig. 4*J*). Given the well-described effects of TGFβ on HSC self-renewal and differentiation (61, 62), these results raise the possibility that altered TGFβ signaling may contribute to the effects of *Tet2* loss-of-function. Overall, these analyses reveal distinct, and sometimes opposite, effects of *Idh2*$^{R172K}$ and *Tet2*$^{-/-}$ on chromatin accessibility in LSK cells.

**Discordant Changes in DNA Methylation and Chromatin Accessibility in *Idh2*$^{R172K}$ Cells.** To identify potential changes in DNA methylation, we performed oxidative reduced representation bisulfite-sequencing (oxBS-seq) on the same cell samples described above. t-SNE analysis indicated that similar to the transcriptome and chromatin accessibility profiles, *Idh2*$^{R172K}$ and *Tet2*$^{-/-}$ cells clustered away from each other and from WT cells, with *Idh2*$^{R172K}$ having a much stronger effect (Fig. 5*A*). *Idh1*$^{R132H}$ and *Idh2*$^{R140Q}$ cells slightly differed from WT cells, associated with several differentially methylated loci (Fig. 5*B* and *SI Appendix*, Fig. S9*C*). Consistently, dot blot analysis of Lin$^{-}$ cells revealed a significant global loss of 5-hmC in *Idh1*$^{R132H}$ and *Idh2*$^{R140Q}$ cells, which was milder than in their *Idh2*$^{R172K}$ and *Tet2*$^{-/-}$ counterparts (Fig. 5*C*). To evaluate which changes may be functionally relevant, we examined differentially methylated CpGs within active LSK enhancers (51). Most altered enhancers were hypermethylated, consistent with data from human AML with *IDH1/2* or *TET2* mutations (21). Changes in *Idh1*$^{R132H}$ and *Idh2*$^{R140Q}$ cells were modest but affected some enhancers located within genes encoding key HSC regulators (*Fli1*, *Hlf*, and *Prmd16*) (*SI Appendix*, Fig. S9 *D–F* and Dataset S3).

To investigate whether changes in chromatin accessibility correlate with altered methylation, we focused on *Idh2*$^{R172K}$ and *Tet2*$^{-/-}$ cells. As expected, closing loci were hypermethylated in both mutants (Fig. 5*D*). Importantly, methylation levels differed within opening chromatin regions in *Idh2*$^{R172K}$ versus *Tet2*$^{-/-}$ cells (Fig. 5*D*). To probe this in more detail, we binned genomic regions into quartiles based on their level of chromatin accessibility. Regardless of genotype, regions with increased accessibility tended to be less methylated (Fig. 5*E*). However, *Idh2*$^{R172K}$ cells consistently displayed hypermethylation compared to the other genotypes across all the accessibility quartiles (Fig. 5*E*). A substantial number of loci were hypermethylated within opening chromatin regions in *Idh2*$^{R172K}$ cells, including at active LSK enhancers (e.g., *Gata2*, *Fli1*, *Pdgfrb*), which never occurred in *Tet2*$^{-/-}$ cells (Fig. 5*F* and Dataset S4). This was true when considering the entire enhancers or only the opening chromatin peaks within them (Fig. 5*F*). Together, these data indicate divergent relationships between chromatin accessibility and DNA methylation changes in *Idh2*$^{R172K}$ versus *Tet2*$^{-/-}$ cells, particularly at opening loci.

We next investigated whether genotype-specific epigenetic changes could be linked to transcriptomic alterations. Given that activating *PDGFRB* rearrangements are oncogenic drivers in myeloid neoplasms (63–65), we further examined the *Pdgfrb* hematopoietic enhancer that selectively gained accessibility despite adjacent hypermethylation in *Idh2*$^{R172K}$ cells (Fig. 6*A*). Integration with ChIP-seq data from LSK cells (51) and HPC-7 mouse progenitors (66, 67) indicated that this site is marked by H3K27ac and H3K4me1 and bound by several hematopoietic regulators that are predicted to have elevated activity in *Idh2*$^{R172K}$ cells, including GATA2, RUNX1, and MEIS1 (Fig. 6*A*). Accordingly, *Pdgfrb* expression and PDGFRB pathway activity were strongly upregulated in *Idh2*$^{R172K}$ cells, whereas the opposite was seen in *Tet2*$^{-/-}$ cells (Fig. 6 *B–D* and *SI Appendix*, Fig. S9*G*). PDGFRB signaling gene sets were also positively enriched in *Idh1*$^{R132H}$ and *Idh2*$^{R140Q}$ mutants (*SI Appendix*, Fig. S9*H*). *Pdgfrb* upregulation in single *Idh2*$^{R172K}$ cells was associated with their abnormal differentiation based on Slingshot analysis (*SI Appendix*, Fig. S7*A*). PDGFRB activates RAS-dependent signaling, a known tumorigenic pathway in AML (68, 69). Consistently, GSEA indicated positive enrichment of RAS pathway components in *Idh2*$^{R172K}$ LSK cells (*SI Appendix*, Fig. S9*G*), associated with upregulation of *Kras*, *Gab1/2*, *Sos2*, *Fyn*, *Src*, and the PDGFRB ligand *Pdgfb* (Fig. 6*B*). By contrast, the expression of these genes was either unchanged or downregulated in *Tet2*$^{-/-}$ cells (Fig. 6*B*). As another example, we noted an *Idh2*$^{R172K}$-specific opening of a chromatin region 3′ to the *Sox4* gene, with features similar to the aforementioned *Pdgfrb* enhancer (Fig. 6*E*). SOX4 is a marker of the malignant progenitor state in human AML (70), can drive self-renewal and differentiation arrest in hematopoietic progenitors and AML cells (71), and predicts poor prognosis in AML patients (72). In our single-cell analyses, Slingshot identified *Sox4* as a main component of the transcriptional program associated with abnormal *Idh2*$^{R172K}$ progenitor differentiation (*SI Appendix*, Fig. S7*A*). SCENIC predicted elevated *Sox4* transcriptional activity in *Idh2*$^{R172K}$ cells (Fig. 3*D*), tracking with increased *Sox4* expression and with the opening of *Sox*-bound chromatin loci (Figs. 4*G* and 6 *B* and *F*). None of these were affected in *Tet2*$^{-/-}$ cells. Overall, these data indicate that mutation-specific epigenetic alterations are associated with aberrant expression and activity of putative drivers of myeloproliferation and impaired differentiation.

## Discussion

Our data showing distinct and opposite effects of *Idh2*$^{R172K}$ and *Tet2*$^{-/-}$ on the transcriptome and epigenome of hematopoietic stem and progenitor cells (*SI Appendix*, Fig. S10) may help to explain some of the clinical distinctions between *IDH1/2* and *TET2* mutated myeloid neoplasms (3, 4). The results raise the

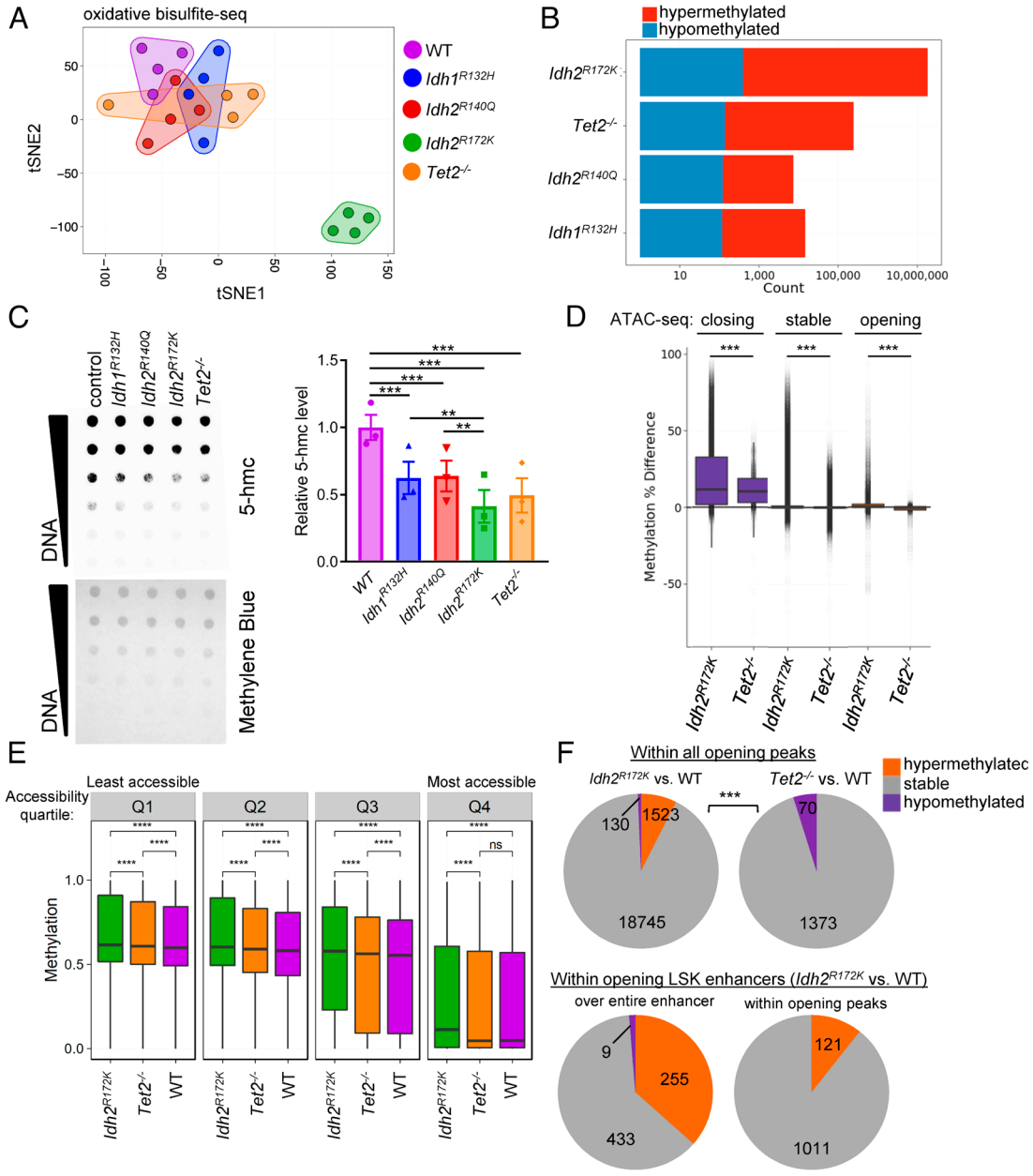


**Fig. 5.** (*A*) t-SNE plot depicting the similarity in overall DNA methylation profile of LSK cells isolated from mice with the indicated genotypes, based on oxBS-seq analysis. Each dot represents an independent sample (biological replicate), each derived from cells pooled from two mice. (*B*) Number of significantly hyper- and hypo-methylated CpGs in LSK cells isolated from mice with the indicated genotypes, compared to wild-type controls. (*C*) Representative dot blot and quantification of three independent biological replicates showing the levels of 5-hmc in $Lin^-$ cells isolated from mice with the indicated genotypes. For quantification, the 5-hmc signal was normalized to total DNA content measured by methylene blue staining of the same membrane. (*D*) Percent methylation changes over genomic area that are opening, closing, or unchanged ($q < 0.05$), determined by the ATAC-seq analyses shown in Fig. 4, in $Idh2^{R172K}$ and $Tet2^{-/-}$ LSK cells compared with wild-type controls. Box plots represent the median and interquartile range. (*E*) Methylation levels over genomic regions binned in accessibility quartiles in LSK cells with the indicated genotypes. Box plots represent the median and interquartile range. (*F*) Distribution of hypomethylated, hypermethylated, or stable loci within all significantly opening chromatin regions in $Idh2^{R172K}$ and $Tet2^{-/-}$ cells and within LSK enhancers in $Idh2^{R172K}$ cells. Data were analyzed using ANOVA with Tukey post hoc tests (*C*), Mann–Whitney tests with Benjamini–Hochberg FDR correction (*D*), Wilcoxon tests with Benjamini–Hochberg FDR correction (*E*), or chi-square test (*F*). $^*P < 0.05$; $^{**}P < 0.01$; $^{***}P < 0.001$.

intriguing possibility that mutual exclusivity between *IDH1/2* and *TET2* lesions in AML (22, 23) could be partially attributable to their antagonistic effects on transcription factor activity and gene expression. Experimentally testing this possibility would be facilitated by the development of disease models that faithfully recapitulate the mutation order and clonal heterogeneity observed in human patients (73). Some of the differences between $Idh2^{R172K}$ and $Tet2^{-/-}$ could be due to the concerted inhibition of multiple α-KG-dependent enzymes by D-2-HG, including histone demethylases (8). Indeed, the occurrences of increased gene expression and chromatin accessibility despite elevated DNA methylation in $Idh2^{R172K}$ cells hint at a potential dominant effect of altered histone regulation, which will be important to examine in further studies. We note that some epigenetic and transcriptomic changes observed in bulk LSK samples may reflect an underlying altered distribution of cell states. However, we clearly observed cases (e.g., *Pdgfrb* and *Sox4*) where expression changes could not readily be linked to the expansion or contraction of specific hematopoietic compartments.

It remains to be clarified whether all the *IDH1/2* mutations have a similar role in mediating oncogenic transformation. Specific *IDH1/2* lesions may have prognostic significance in patients, although this is controversial (74), differs greatly between studies

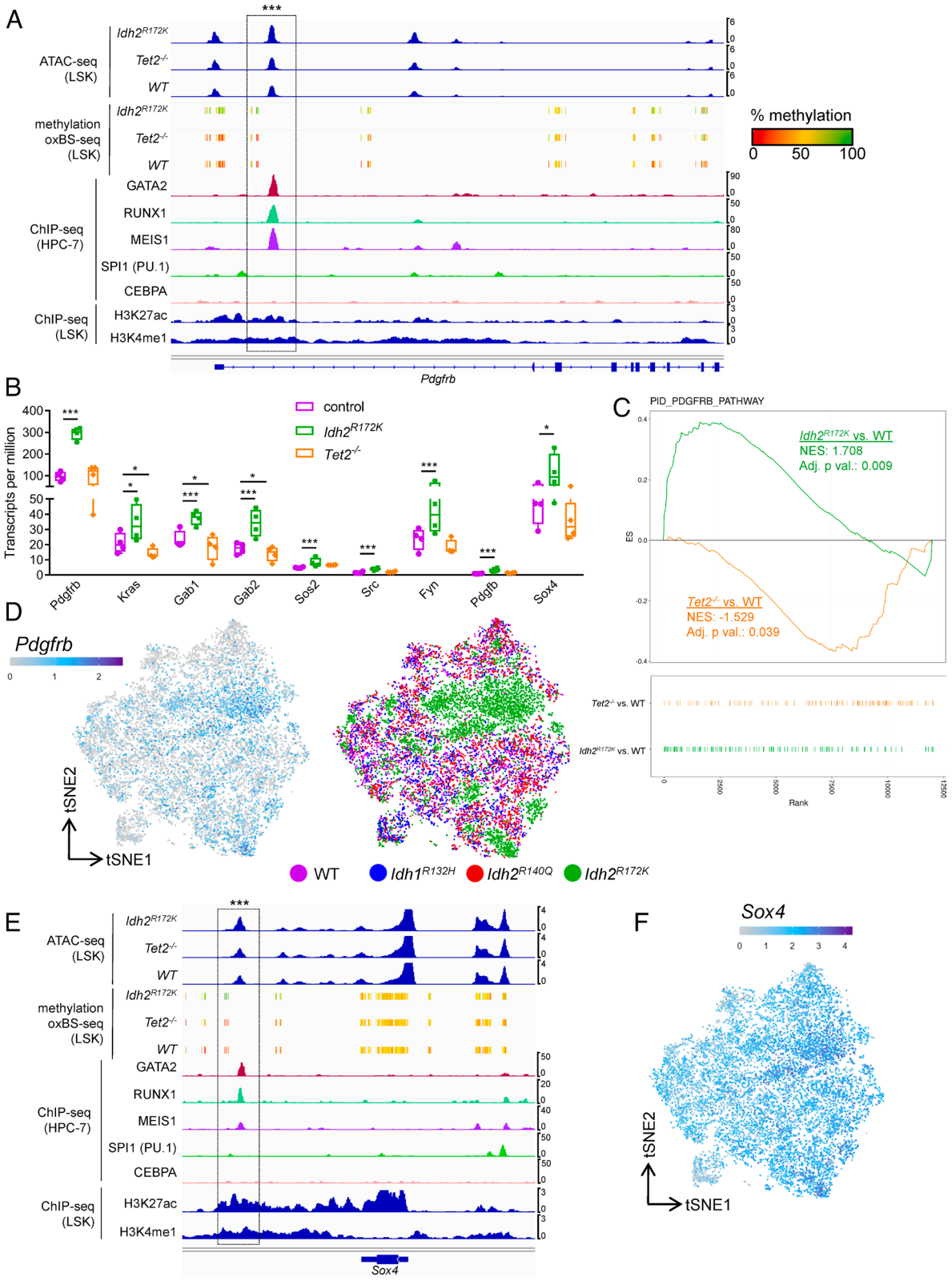


**Fig. 6.** (*A*) Tracks representing the normalized average chromatin accessibility (determined by ATAC-seq) and DNA methylation (determined by oxBS-seq) near the *Pdgfrb* gene in LSK cells isolated from mice with the indicated genotypes. Tracks depicting the binding of selected transcription factors or histone marks, derived from published chromatin immunoprecipitation experiments in HPC-7 or LSK cells, were aligned to the ATAC-seq and oxBS-seq tracks. A differentially accessible peak of interest is boxed. (*B*) Relative expression of the indicated genes, determined by RNA-seq analysis, in LSK cells isolated from mice with the indicated genotypes. Each dot represents an individual sample. (*C*) GSEA plots depicting the relative expression of PDGFRB signaling pathway genes in *Idh2*$^{R172K}$ and *Tet2*$^{-/-}$ LSK bone marrow cells, compared to their wild-type counterparts, based on RNA-sequencing data. (*D*) Relative expression (z-scored) of *Pdgfrb* in single LSK bone marrow cells, overlaid on the t-SNE plot presented in Fig. 3*C* and reproduced here to highlight single-cell genotypes. (*E*) Tracks representing the normalized average chromatin accessibility (determined by ATAC-seq) and DNA methylation (determined by oxBS-seq) near the *Sox4* gene in LSK cells isolated from mice with the indicated genotypes. Tracks depicting the binding of selected transcription factors or histone marks, derived from published chromatin immunoprecipitation experiments in HPC-7 or LSK cells, were aligned to the ATAC-seq and oxBS-seq tracks. A differentially accessible peak of interest is boxed. (*F*) Relative expression (z-scored) of *Sox4* in single LSK bone marrow cells, overlaid on the t-SNE plot presented in Fig. 3 and reproduced in panel *C* to highlight single-cell genotypes.

(3, 4, 9, 29, 75–80), and may be influenced by several factors such as co-occurring mutations and patient age (9, 78, 79). Differences in isoform localization (IDH1 in the cytoplasm versus IDH2 in the mitochondria) may result in mutation-specific alterations in metabolism that will be important to address in future studies (81–83). Nevertheless, given that *Idh2*$^{R172K}$ and *Idh2*$^{R140Q}$ mice are genetically identical except for their respective point mutation, it is clear that the higher level of D-2-HG in *Idh2*$^{R172K}$ cells is a key determinant of phenotype severity. This could explain the unique genomic profile of *IDH2*$^{R172}$ AMLs, characterized by fewer mutations compared to *IDH1*$^{R132}$ and *IDH2*$^{R140}$ diseases (4, 29, 31, 84). Higher D-2-HG production by *IDH2*$^{R172}$ could activate oncogenic pathways that normally require second-hit mutations in *IDH1*$^{R132}$ and *IDH2*$^{R140}$ AMLs, such as RAS signaling as we observe here (29).

Mutant IDH inhibitors have demonstrated substantial clinical efficacy (31–33). Importantly, these drugs induce leukemic cell differentiation, rather than cell death or proliferation arrest (37, 84). In some patients, this can be associated with the development of clinically significant "differentiation syndrome" (85, 86). In addition, resistance to IDH inhibitors can emerge from leukemic clones that retain *IDH1/2* mutations and acquire new lesions (37). Therefore, it may be beneficial to target the growth or maintenance of *IDH1/2*-mutated leukemic cells in combination with differentiation induction. Given that RAS/RTK pathway mutations have been associated with resistance to IDH inhibitors (84, 87), it was interesting to identify PDGF/RAS signaling as a possible contributor to myeloproliferation in *Idh2*$^{R172K}$ mice, paralleling prior observations in *IDH*-mutated AML (88). Future studies could investigate the effects of cotargeting mutant IDH and PDGF/RAS signaling. This and other approaches informed by a better understanding of genotype-specific oncogenic mechanisms may help to develop improved therapies.

## Materials and Methods

A detailed description of *Materials and Methods* is provided in *SI Appendix, Supplementary Materials and Methods*.

**Mice.** The *Idh1*$^{LSL\text{-}R132H}$, *Idh2*$^{LSL\text{-}R140Q}$, and *Idh2*$^{LSL\text{-}R172K}$ alleles were generated by inserting a *loxP*-flanked STOP cassette in the third intron and point mutations in exon 4 (89). *Tet2*$^{-/-}$ mice (JAX #23359) and Vav-Cre (JAX #008610) have been described previously (43, 90). All mouse strains were backcrossed to a C57BL/6J background for >10 generations. Animal experiments were performed in accordance with institutional and federal guidelines and were approved by an animal care committee (University Health Network, protocol #985).

**Cell Isolation and Flow Cytometry.** Bone marrow cells were isolated by flushing in cold MACS buffer (phosphate-buffered saline with 0.5% bovine serum albumin and 2 mM EDTA pH8.0). The spleen and thymus were crushed through a 70-μm nylon mesh in a cold buffer. Following red blood cell lysis, cells were counted and resuspended at the appropriate dilution for further processing. Colony-forming assays were performed in MethoCult GF M3434 methylcellulose medium (STEMCELL Technologies) following the manufacturer's protocol. Lineage-negative cells were enriched using the Mouse Lineage Cell Depletion Kit (Miltenyi Biotec #130-090-858), according to the manufacturer's instructions and using an AutoMACS Pro instrument (Miltenyi Biotec). For CYTOF, lineage-negative cells were stained with metal-tagged antibodies and 500 nM IdU to label newly synthesized DNA as previously described (91). All antibodies and staining conditions are described in *SI Appendix, Supplementary Methods*.

**RNA-seq, ATAC-seq, and RRoxBS-seq Analyses.** For multiomic profiling, RNA and DNA were extracted from 1 × $10^5$ LSK cells (two animals pooled per biological replicate) using the AllPrep DNA/RNA Micro Kit (Qiagen #80284). For ATAC-seq, the OMNI-ATAC method was used on 5 × $10^4$ cells (92). Detailed procedures are provided in *SI Appendix, Supplementary Methods*. Library preparation, sequencing, and data acquisition were performed at the Weill Cornell Medicine Epigenomics Core as previously described (93, 94). The bioinformatics pipelines to analyze RNA-seq (94), ATAC-seq (95), and RRoxBS-seq (96) followed previously described approaches and are detailed in *SI Appendix, Supplementary Methods*. For single-cell RNA-seq, LSK cells were loaded on a 10× single cell A chip and processed using Single Cell 3′ Reagent Kits v2 for single-cell capturing and mRNA barcoding (10x Genomics). cDNA libraries were prepared using the Chromium Single-Cell 3′ Library Kit and Gel Bead Kit v2 and i7 Multiplex Kit (10X Genomics) and sequenced on an Illumina HiSeq 2500 system in 2 × 150 bp paired-end mode. The raw sequencing reads were first processed and mapped to mouse genome build GRCm38 using the CellRanger software (v2.1.0, 10X Genomics), followed by analysis using Seurat (47, 97), SCENIC (45), and Slingshot (46) as detailed in *SI Appendix, Supplementary Methods*. Data are available in Gene Expression Omnibus (Bulk RNA-seq, ATAC-seq, and RRoxBS-seq: GSE204941(98). Single-cell RNA-seq: GSE202696(99)).

**Data, Materials, and Software Availability.** Data are available in Gene Expression Omnibus (Bulk RNA-seq, ATAC-seq, and RRoxBS-seq: GSE204941. Single-cell RNA-seq: GSE202696).

**ACKNOWLEDGMENTS.** This work was supported by a Specialized Center of Research grant from the Leukemia and Lymphoma Society (LLS-SCOR grant) to T.W.M., C.M., A.M., C.J.G., and R.L.L. J.Fortin was supported by a Next Generation of Scientist grant from the Cancer Research Society. We thank the Princess Margaret Genomics Centre, the Weill Cornell Medicine Epigenomics Core Facility, and the Integrated Genomics Operation (IGO) core at the Sloan Kettering Institute for support.

Author affiliations: [a]Princess Margaret Cancer Centre, University Health Network, Toronto, ON M5G 2C1, Canada; [b]Department of Physiology and Biophysics, Weill Cornell Medicine, New York, NY 10065; [c]The HRH Prince Alwaleed Bin Talal Bin Abdulaziz Al-Saud Institute for Computational Biomedicine, Weill Cornell Medicine, New York, NY 10065; [d]WorldQuant Initiative for Quantitative Prediction, Weill Cornell Medicine, New York, NY 10065; [e]Institut Mondor de Recherche Biomédicale, INSERMU955, Université Paris Est Créteil, Créteil 94010, France; [f]Centre for Oncology and Immunology, Hong Kong Science Park, Hong Kong SAR, China; [g]Department of Immunology, The Hospital for Sick Children Research Institute, University of Toronto, Toronto, ON M5G 0A4, Canada; [h]Department of Hematology and Oncology, Graduate School of Medicine, Kyoto University, Kyoto 606-8501, Japan; [i]Human Oncology and Pathogenesis Program, Memorial Sloan Kettering Cancer Center, New York, NY 10065; [j]Louis V. Gerstner, Jr. Graduate School of Biomedical Sciences, Memorial Sloan Kettering Cancer Center, New York, NY 10065; [k]Center for Epigenetics Research, Memorial Sloan Kettering Cancer Center, New York, NY 10065; [l]Center for Hematologic Malignancies, Memorial Sloan Kettering Cancer Center, New York, NY 10065; [m]Department of Medicine, Division of Hematology and Medical Oncology, Weill Cornell Medicine, New York, NY 10021; and [n]Department of Pathology, School of Clinical Medicine, Li Ka Shing Faculty of Medicine, The University of Hong Kong, Hong Kong SAR, China

1. A. S. Sperling, C. J. Gibson, B. L. Ebert, The genetics of myelodysplastic syndrome: From clonal haematopoiesis to secondary leukaemia. *Nat. Rev. Cancer* **17**, 5–19 (2017).
2. A. Khwaja *et al.*, Acute myeloid leukaemia. *Nat. Rev. Dis. Primers* **2**, 16010 (2016).
3. E. Papaemmanuil *et al.*, Genomic classification and prognosis in acute myeloid leukemia. *N. Engl. J. Med.* **374**, 2209–2221 (2016).
4. J. P. Patel *et al.*, Prognostic relevance of integrated genetic profiling in acute myeloid leukemia. *N. Engl. J. Med.* **366**, 1079–1089 (2012).
5. R. L. Bowman, L. Busque, R. L. Levine, Clonal hematopoiesis and evolution to hematopoietic malignancies. *Cell Stem Cell* **22**, 157–170 (2018).
6. A. H. Shih, O. Abdel-Wahab, J. P. Patel, R. L. Levine, The role of mutations in epigenetic regulators in myeloid malignancies. *Nat. Rev. Cancer* **12**, 599–612 (2012).
7. C. D. DiNardo *et al.*, IDH1 and IDH2 mutations in myelodysplastic syndromes and role in disease progression. *Leukemia* **30**, 980–984 (2016).
8. R. A. Cairns, T. W. Mak, Oncogenic isocitrate dehydrogenase mutations: Mechanisms, models, and clinical opportunities. *Cancer Discov.* **3**, 730–741 (2013).
9. G. Marcucci *et al.*, IDH1 and IDH2 gene mutations identify novel molecular subsets within de novo cytogenetically normal acute myeloid leukemia: A cancer and leukemia group B study. *J. Clin. Oncol.* **28**, 2348–2355 (2010).
10. E. R. Mardis *et al.*, Recurring mutations found by sequencing an acute myeloid leukemia genome. *N. Engl. J. Med.* **361**, 1058–1066 (2009).
11. P. S. Ward *et al.*, The common feature of leukemia-associated IDH1 and IDH2 mutations is a neomorphic enzyme activity converting alpha-ketoglutarate to 2-hydroxyglutarate. *Cancer Cell* **17**, 225–234 (2010).
12. L. Dang *et al.*, Cancer-associated IDH1 mutations produce 2-hydroxyglutarate. *Nature* **462**, 739–744 (2009).
13. M. E. Figueroa *et al.*, Leukemic IDH1 and IDH2 mutations result in a hypermethylation phenotype, disrupt TET2 function, and impair hematopoietic differentiation. *Cancer Cell* **18**, 553–567 (2010).
14. W. Xu *et al.*, Oncometabolite 2-hydroxyglutarate is a competitive inhibitor of alpha-ketoglutarate-dependent dioxygenases. *Cancer Cell* **19**, 17–30 (2011).
15. R. L. Bowman, R. L. Levine, TET2 in normal and malignant hematopoiesis. *Cold Spring Harb. Perspect. Med.* **7**, a026518 (2017).
16. L. Busque *et al.*, Recurrent somatic TET2 mutations in normal elderly individuals with clonal hematopoiesis. *Nat. Genet.* **44**, 1179–1181 (2012).
17. F. Delhommeau *et al.*, Mutation in TET2 in myeloid cancers. *N. Engl. J. Med.* **360**, 2289–2301 (2009).
18. A. M. Jankowska *et al.*, Loss of heterozygosity 4q24 and TET2 mutations associated with myelodysplastic/myeloproliferative neoplasms. *Blood* **113**, 6403–6410 (2009).

19. S. M. Langemeijer *et al.*, Acquired mutations in TET2 are common in myelodysplastic syndromes. *Nat. Genet.* **41**, 838–842 (2009).
20. A. Tefferi *et al.*, TET2 mutations and their clinical correlates in polycythemia vera, essential thrombocythemia and myelofibrosis. *Leukemia* **23**, 905–911 (2009).
21. E. R. Wilson *et al.*, Focal disruption of DNA methylation dynamics at enhancers in IDH-mutant AML cells. *Leukemia* **36**, 935–945 (2022).
22. L. A. Miles *et al.*, Single-cell mutation analysis of clonal evolution in myeloid malignancies. *Nature* **587**, 477–482 (2020).
23. K. Morita *et al.*, Clonal evolution of acute myeloid leukemia revealed by high-throughput single-cell genomics. *Nat. Commun.* **11**, 5327 (2020).
24. S. M. Chan *et al.*, Isocitrate dehydrogenase 1 and 2 mutations induce BCL-2 dependence in acute myeloid leukemia. *Nat. Med.* **21**, 178–184 (2015).
25. G. Genovese *et al.*, Clonal hematopoiesis and blood-cancer risk inferred from blood DNA sequence. *N. Engl. J. Med.* **371**, 2477–2487 (2014).
26. S. Jaiswal *et al.*, Age-related clonal hematopoiesis associated with adverse outcomes. *N. Engl. J. Med.* **371**, 2488–2498 (2014).
27. R. A. Cairns *et al.*, IDH2 mutations are frequent in angioimmunoblastic T-cell lymphoma. *Blood* **119**, 1901–1903 (2012).
28. F. Lemonnier *et al.*, Recurrent TET2 mutations in peripheral T-cell lymphomas correlate with TFH-like features and adverse clinical parameters. *Blood* **120**, 1466–1469 (2012).
29. M. Meggendorfer *et al.*, IDH1R132, IDH2R140 and IDH2R172 in AML: Different genetic landscapes correlate with outcome and may influence targeted treatment strategies. *Leukemia* **32**, 1249–1253 (2018).
30. P. S. Ward *et al.*, The potential for isocitrate dehydrogenase mutations to produce 2-hydroxyglutarate depends on allele specificity and subcellular compartmentalization. *J. Biol. Chem.* **288**, 3804–3815 (2013).
31. C. D. DiNardo *et al.*, Durable remissions with ivosidenib in IDH1-mutated relapsed or refractory AML. *N. Engl. J. Med.* **378**, 2386–2398 (2018).
32. E. M. Stein *et al.*, Ivosidenib or enasidenib combined with intensive chemotherapy in patients with newly diagnosed AML: A phase 1 study. *Blood* **137**, 1792–1803 (2021).
33. E. M. Stein *et al.*, Enasidenib in mutant IDH2 relapsed or refractory acute myeloid leukemia. *Blood* **130**, 722–731 (2017).
34. S. Choe *et al.*, Molecular mechanisms mediating relapse following ivosidenib monotherapy in IDH1-mutant relapsed or refractory AML. *Blood Adv.* **4**, 1894–1905 (2020).
35. J. J. Harding *et al.*, Isoform switching as a mechanism of acquired resistance to mutant isocitrate dehydrogenase inhibition. *Cancer Discov.* **8**, 1540–1547 (2018).
36. A. M. Intlekofer *et al.*, Acquired resistance to IDH inhibition through trans or cis dimer-interface mutations. *Nature* **559**, 125–129 (2018).
37. L. Quek *et al.*, Clonal heterogeneity of acute myeloid leukemia treated with the IDH2 inhibitor enasidenib. *Nat. Med.* **24**, 1167–1177 (2018).
38. K. Ito *et al.*, Non-catalytic roles of Tet2 are essential to regulate hematopoietic stem and progenitor cell homeostasis. *Cell Rep.* **28**, 2480–2490 e2484 (2019).
39. K. Moran-Crusio *et al.*, Tet2 loss leads to increased hematopoietic stem cell self-renewal and myeloid transformation. *Cancer Cell* **20**, 11–24 (2011).
40. C. Quivoron *et al.*, TET2 inactivation results in pleiotropic hematopoietic abnormalities in mouse and is a recurrent event during human lymphomagenesis. *Cancer Cell* **20**, 25–38 (2011).
41. Z. Zhao *et al.*, Combined loss of Tet1 and Tet2 promotes B cell, but not myeloid malignancies, in mice. *Cell Rep.* **13**, 1692–1704 (2015).
42. S. Inoue *et al.*, Mutant IDH1 downregulates ATM and alters DNA repair and sensitivity to DNA damage independent of TET2. *Cancer Cell* **30**, 337–348 (2016).
43. M. Ko *et al.*, Ten-Eleven-Translocation 2 (TET2) negatively regulates homeostasis and differentiation of hematopoietic stem cells in mice. *Proc. Natl. Acad. Sci. U.S.A.* **108**, 14566–14571 (2011).
44. F. Izzo *et al.*, DNA methylation disruption reshapes the hematopoietic differentiation landscape. *Nat. Genet.* **52**, 378–387 (2020).
45. S. Aibar *et al.*, SCENIC: Single-cell regulatory network inference and clustering. *Nat. Methods* **14**, 1083–1086 (2017).
46. K. Street *et al.*, Slingshot: Cell lineage and pseudotime inference for single-cell transcriptomics. *BMC Genomics* **19**, 477 (2018).
47. T. Stuart *et al.*, Comprehensive integration of single-cell data. *Cell* **177**, 1888–1902.e1821 (2019).
48. C. Barletta, P. G. Pelicci, L. C. Kenyon, S. D. Smith, R. Dalla-Favera, Relationship between the c-myb locus and the 6q-chromosomal aberration in leukemias and lymphomas. *Science* **235**, 1064–1067 (1987).
49. Y. K. Lieu, E. P. Reddy, Conditional c-myb knockout in adult hematopoietic stem cells leads to loss of self-renewal due to impaired proliferation and accelerated differentiation. *Proc. Natl. Acad. Sci. U.S.A.* **106**, 21689–21694 (2009).
50. P. G. Pelicci, L. Lanfrancone, M. D. Brathwaite, S. R. Wolman, R. Dalla-Favera, Amplification of the c-myb oncogene in a case of human acute myelogenous leukemia. *Science* **224**, 1117–1121 (1984).
51. B. Aranda-Orgilles *et al.*, MED12 regulates HSC-specific enhancers independently of mediator kinase activity to control hematopoiesis. *Cell Stem Cell* **19**, 784–799 (2016).
52. E. H. Bresnick, K. D. Johnson, Blood disease-causing and -suppressing transcriptional enhancers: General principles and GATA2 mechanisms. *Blood Adv.* **3**, 2045–2056 (2019).
53. K. D. Johnson *et al.*, Cis-element mutated in GATA2-dependent immunodeficiency governs hematopoiesis and vascular integrity. *J. Clin. Invest.* **122**, 3692–3704 (2012).
54. K. D. Johnson *et al.*, Cis-regulatory mechanisms governing stem and progenitor cell transitions. *Sci. Adv.* **1**, e1500503 (2015).
55. Q. F. Wang *et al.*, Regulation of MEIS1 by distal enhancer elements in acute leukemia. *Leukemia* **28**, 138–146 (2014).
56. P. Xiang *et al.*, Delineating MEIS1 cis-regulatory elements active in hematopoietic cells. *Leukemia* **28**, 433–436 (2014).
57. F. Aguilo *et al.*, Prdm16 is a physiologic regulator of hematopoietic stem cells. *Blood* **117**, 5057–5066 (2011).
58. S. Chuikov, B. P. Levi, M. L. Smith, S. J. Morrison, Prdm16 promotes stem cell maintenance in multiple tissues, partly by regulating oxidative stress. *Nat. Cell Biol.* **12**, 999–1006 (2010).
59. K. O. Gudmundsson *et al.*, Prdm16 is a critical regulator of adult long-term hematopoietic stem cell quiescence. *Proc. Natl. Acad. Sci. U.S.A.* **117**, 31945–31953 (2020).
60. L. Brunetti *et al.*, Mutant NPM1 maintains the leukemic state through HOX expression. *Cancer Cell* **34**, 499–512.e9 (2018).
61. G. A. Challen, N. C. Boles, S. M. Chambers, M. A. Goodell, Distinct hematopoietic stem cell subtypes are differentially regulated by TGF-beta1. *Cell Stem Cell* **6**, 265–278 (2010).
62. X. Wang *et al.*, TGF-beta1 negatively regulates the number and function of hematopoietic stem cells. *Stem Cell Rep.* **11**, 274–287 (2018).
63. J. F. Apperley *et al.*, Response to imatinib mesylate in patients with chronic myeloproliferative diseases with rearrangements of the platelet-derived growth factor receptor beta. *New Engl. J. Med.* **347**, 481–487 (2002).
64. M. Arefi *et al.*, Incidence and clinical characteristics of myeloproliferative neoplasms displaying a PDGFRB rearrangement. *Eur. J. Haematol.* **89**, 37–41 (2012).
65. T. R. Golub, G. F. Barker, M. Lovett, D. G. Gilliland, Fusion of PDGF receptor beta to a novel ets-like gene, tel, in chronic myelomonocytic leukemia with t(5;12) chromosomal translocation. *Cell* **77**, 307–316 (1994).
66. N. K. Wilson *et al.*, Combinatorial transcriptional control in blood stem/progenitor cells: Genome-wide analysis of ten major transcriptional regulators. *Cell Stem Cell* **7**, 532–544 (2010).
67. N. K. Wilson *et al.*, Integrated genome-scale analysis of the transcriptional regulatory landscape in a blood stem/progenitor cell model. *Blood* **127**, e12–23 (2016).
68. J. Andrae, R. Gallini, C. Betsholtz, Role of platelet-derived growth factors in physiology and medicine. *Genes Dev.* **22**, 1276–1312 (2008).
69. A. F. Ward, B. S. Braun, K. M. Shannon, Targeting oncogenic Ras signaling in hematologic malignancies. *Blood* **120**, 3397–3406 (2012).
70. P. van Galen *et al.*, Single-cell RNA-seq reveals AML hierarchies relevant to disease progression and immunity. *Cell* **176**, 1265–1281.e24 (2019).
71. H. Zhang *et al.*, Sox4 is a key oncogenic target in C/EBPalpha mutant acute myeloid leukemia. *Cancer Cell* **24**, 575–588 (2013).
72. J. W. Lu *et al.*, Overexpression of SOX4 correlates with poor prognosis of acute myeloid leukemia and is leukemogenic in zebrafish. *Blood Cancer J.* **7**, e593 (2017).
73. B. A. Benard *et al.*, Clonal architecture predicts clinical outcomes and drug sensitivity in acute myeloid leukemia. *Nat. Commun.* **12**, 7244 (2021).
74. B. C. Medeiros *et al.*, Isocitrate dehydrogenase mutations in myeloid malignancies. *Leukemia* **31**, 272–281 (2017).
75. N. Boissel *et al.*, Differential prognosis impact of IDH2 mutations in cytogenetically normal acute myeloid leukemia. *Blood* **117**, 3696–3697 (2011).
76. C. L. Green *et al.*, The prognostic significance of IDH2 mutations in AML depends on the location of the mutation. *Blood* **118**, 409–412 (2011).
77. M. Duchmann *et al.*, Prognostic significance of concurrent gene mutations in intensively treated patients with IDH-mutated AML: An ALFA study. *Blood* **137**, 2827–2837 (2021).
78. P. Paschka *et al.*, IDH1 and IDH2 mutations are frequent genetic alterations in acute myeloid leukemia and confer adverse prognosis in cytogenetically normal acute myeloid leukemia with NPM1 mutation without FLT3 internal tandem duplication. *J. Clin. oncol.* **28**, 3636–3643 (2010).
79. F. Thol *et al.*, Prognostic impact of IDH2 mutations in cytogenetically normal acute myeloid leukemia. *Blood* **116**, 614–616 (2010).
80. K. Willander *et al.*, Mutations in the isocitrate dehydrogenase 2 gene and IDH1 SNP 105C > T have a prognostic value in acute myeloid leukemia. *Biomarker Res.* **2**, 18 (2014).
81. J. A. Losman, W. G. Kaelin Jr., What a difference a hydroxyl makes: Mutant IDH, (R)-2-hydroxyglutarate, and cancer. *Genes Dev.* **27**, 836–852 (2013).
82. S. K. McBrayer *et al.*, Transaminase inhibition by 2-hydroxyglutarate impairs glutamate biosynthesis and redox homeostasis in glioma. *Cell* **175**, 101–116.e25 (2018).
83. S. J. Parker, C. M. Metallo, Metabolic consequences of oncogenic IDH mutations. *Pharmacol. Ther.* **152**, 54–62 (2015).
84. M. D. Amatangelo *et al.*, Enasidenib induces acute myeloid leukemia cell differentiation to promote clinical response. *Blood* **130**, 732–741 (2017).
85. A. T. Fathi *et al.*, Differentiation syndrome associated with enasidenib, a selective inhibitor of mutant isocitrate dehydrogenase 2: Analysis of a phase 1/2 study. *JAMA Oncol.* **4**, 1106–1110 (2018).
86. K. J. Norsworthy *et al.*, Differentiation syndrome with ivosidenib and enasidenib treatment in patients with relapsed or refractory IDH-mutated AML: A U.S. food and drug administration systematic analysis. *Clin. Cancer Res.* **26**, 4280–4288 (2020).
87. F. Wang *et al.*, Leukemia stemness and co-occurring mutations drive resistance to IDH inhibitors in acute myeloid leukemia. *Nat. Commun.* **12**, 2607 (2021).
88. J. L. Glass *et al.*, Epigenetic identity in AML depends on disruption of nonpromoter regulatory elements and is affected by antagonistic effects of mutations in epigenetic modifiers. *Cancer Dis.* **7**, 868–883 (2017).
89. F. Lemonnier *et al.*, The IDH2 R172K mutation associated with angioimmunoblastic T-cell lymphoma produces 2HG in T cells and impacts lymphoid development. *Proc. Natl. Acad. Sci. U.S.A.* **113**, 15084–15089 (2016).
90. J. de Boer *et al.*, Transgenic mice with hematopoietic and lymphoid specific expression of Cre. *Eur. J. Immunol.* **33**, 314–325 (2003).
91. M. A. Galati *et al.*, Cancers from novel pole-mutant mouse models provide insights into polymerase-mediated hypermutagenesis and immune checkpoint blockade. *Cancer Res.* **80**, 5606–5618 (2020).
92. M. R. Corces *et al.*, An improved ATAC-seq protocol reduces background and enables interrogation of frozen tissues. *Nat. Methods* **14**, 959–962 (2017).
93. J. D. Buenrostro, B. Wu, H. Y. Chang, W. J. Greenleaf, ATAC-seq: A method for assaying chromatin accessibility genome-wide. *Curr. Protoc. Mol. Biol.* **109**, 21–31 (2015).
94. W. Beguelin *et al.*, Mutant EZH2 induces a pre-malignant lymphoma niche by reprogramming the immune response. *Cancer Cell* **37**, 655–67.e11 (2020).
95. K. Hatzi *et al.*, Histone demethylase LSD1 is required for germinal center formation and BCL6-driven lymphomagenesis. *Nat. Immunol.* **20**, 86–96 (2019).
96. A. H. Shih *et al.*, Combination targeted therapy to disrupt aberrant oncogenic signaling and reverse epigenetic dysfunction in IDH2- and TET2-mutant acute myeloid leukemia. *Cancer Dis.* **7**, 494–505 (2017).
97. A. Butler, P. Hoffman, P. Smibert, E. Papalexi, R. Satija, Integrating single-cell transcriptomic data across different conditions, technologies, and species. *Nat. Biotechnol.* **36**, 411–420 (2018).
98. J. Fortin *et al.*, Distinct and opposite effects of leukemogenic Idh and Tet2 mutations in hematopoietic stem and progenitor cells. *Gene Expression Omnibus*, https://www.ncbi.nlm.nih.gov/geo/query/acc.cgi?acc=GSE204941. May 26, 2022
99. J. Fortin *et al.*, Distinct and opposite effects of leukemogenic Idh and Tet2 mutations in hematopoieticstem and progenitor cells. *Gene Expression Omnibus*, https://www.ncbi.nlm.nih.gov/geo/query/acc.cgi?acc=GSE202696. May 13, 2022